Temperature resistant fast In$_x$Ga$_{1-x}$As / GaAs quantum dot saturable absorber for the epitaxial integration into semiconductor surface emitting lasers

T. FINKE,[1] J. NÜRNBERG,[2] V. SICHKOVSKYI,[1] M. GOLLING,[2] U. KELLER,[2] AND J. P. REITHMAIER[1]

[1]*Technische Physik, Institute of Nanostructure Technologies and Analytics (INA), Center for Interdisciplinary Nanostructure Science and Technology (CINSaT), University of Kassel, Heinrich-Plett-Straße 40, 34132 Kassel, Germany*
[2]*Department of Physics, Institute of Quantum Electronics, ETH Zurich, Wolfgang-Pauli-Str. 16, 8093 Zurich, Switzerland*
tanja.finke@ina.uni-kassel.de

Abstract: Quantum-dot-based semiconductor saturable absorber mirrors (SESAMs) with fast response times were developed by molecular beam epitaxy (MBE). Using quantum dots (QDs) in the absorber region of the SESAMs instead of quantum wells, enables additional degrees of freedom in the design, the control of saturation parameters and the recovery dynamics. However, if one wants to integrate such a SESAM element into semiconductor surface emitting lasers such as a mode-locked integrated external-cavity surface-emitting laser (MIXSEL), the saturable absorber layers have to withstand a longer high-temperature growth procedure for the epitaxial formation of distributed Bragg reflectors (DBR). Typically defect related SESAMs will be annealed at those growth temperatures and lose their high-speed performance. Here we present a systematic study on the growth parameters and post-growth annealing of SESAMs based on high-quality In$_x$Ga$_{1-x}$As/GaAs quantum dots (QDs) grown by MBE at growth temperatures of 450 °C or higher. The good quality enables the QDs to survive the long DBR overgrowth at 600 °C with only minimal shifts in the designed operation wavelength of 1030 nm required for growth of MIXSEL devices. The introduction of recombination centers with p-type modulation doping and additional post-growth annealing improves the absorption of the high-quality QDs. Hence, low saturation fluences < 10 μJ/cm^2 and a reduction of the $\tau_{1/e}$ recovery time to values < 2 ps can be achieved.

1. Introduction

Since its invention in 1992, semiconductor saturable absorber mirrors (SESAMs) [1] have been well established for passive mode-locking of different laser types from diode-pumped solid-state [2], fiber [3] and surface emitting semiconductor disk lasers [4,5]. Due to its design flexibility, the SESAM enables operation over a wide range of pulse durations and repetition rates. The average power can range from a few mW up to several 100 W at wavelengths from the visible to the infrared. A SESAM consists of a high-quality distributed Bragg reflector (DBR) followed by a quantum well (QW) or quantum dot (QD) absorber region. The design of the DBR and the active region is adapted and optimized for the desired optical parameters, such as the operation wavelength λ, the modulation depth ΔR, the saturation fluence F_{sat}, the non-saturable losses ΔR_{ns}, and the recovery time τ [6]. SESAMs for stable mode-locking of optically pumped semiconductor disk laser require low saturation fluences (< 10 μJ/cm^2) [7] and can easily provide high repetition rates (> 10 GHz) [8] without Q-switching instabilities.

The QD-SESAMs presented in this paper are developed for faster saturable absorbers that are more robust even with additional annealing during a longer epitaxial growth process. Such absorbers are required for shorter pulse generation from mode-locked optically pumped surface emitting semiconductor disc lasers, especially for the integration in mode-locked integrated external-cavity surface-emitting lasers (MIXSELs) [9]. A passively mode-locked semiconductor laser exhibits a dynamic pulse-to-pulse gain saturation and therefore requires a saturable absorber that needs to saturate and recover faster than the gain [4].

To date, most SESAMs are based on QW absorber sections. Nevertheless, QD-SESAMs have already shown high potential and have been applied for passively mode-locked diode-pumped solid-state lasers [10], vertical external cavity surface-emitting lasers (VECSELs) [11–13] and MIXSELs [14]. However, the integration of low-temperature grown SESAMs in a monolithically grown MIXSEL structure is very challenging due to the high-temperature long-term overgrowth at 550–610 °C needed for the thick DBR. The defects will be annealed at a high percentage and also the composition and size of the QDs may change [14,15]. This substantially increased the QD saturable absorber recovery time and therefore the mode-locked pulse duration. Femtosecond pulses from a MIXSEL were only achieved with a single low-temperature grown InGaAs QW embedded in AlAs spacer layers and operated close to the QW bandedge to obtain a faster absorber saturation compared to the gain [16]. The defects in the AlAs barrier layers turned out to be more robust even with long annealing times. However, these QW-MIXSELs exhibit stronger temperature sensitivity [17].

The motivation behind the use of QDs saturable absorbers is the ability to tailor the optical properties over a wide range by exploiting additional geometry-based degrees of freedom [15,18]. They help to optimize the various parameters: the absorption wavelength can be adjusted with different QD sizes; the modulation depth can be easily regulated by changing the QD density or number of QD layers. Furthermore, the typical inhomogeneous linewidth broadening leads to a broader absorption range [19]. High temperature grown InAs QD-SESAMs operating in the 1.55 µm range have been shown in 2019 [20]. But all previously studied QD-absorbers operating in the 1-µm range consist of self-assembled InAs QD layers grown at temperatures below 400 °C. This leads to an increased number of growth-related defects, especially arsenic-anti-site point defects [21,22], which would not be desirable for any active gain medium, but have shown to be useful for saturable absorbers [23–25]. The presence of such defects enhances the absorption mechanism by providing more fast non-radiative recombination channels. Accordingly, the recovery time can be strongly reduced for QD-SESAMs grown at low temperature [15,25,26].

The optical quality of InAs or InGaAs QDs improves with growth temperatures above 430 °C, which is measurable by increased photoluminescence intensities [19,27]. To counteract the thermally induced wavelength shift of QDs during growth and to achieve more temperature-insensitive recovery dynamics, a new approach for the realization of QD-SESAMs is presented in this paper. Instead of non-radiative recombination centers, the radiative recombination is enhanced by a p-type δ-doping, which generates a high hole density in QDs by modulation doping. This allows faster recombination and can reduce the slow component of the recovery dynamics, because no hole transport is needed anymore, and the hole density can be kept constantly high although the electron density gets low on longer time scales. The effect of p-doping should not be mixed with the positive effect of p-doping of low-temperature grown GaAs absorbers. There, the p-doping improves the performance due to the reduction of density of neutral anti-site defects (As_{Ga}^0) concentration in comparison to charged ones (As_{Ga}^+) [24,25] and has nothing to do with the enhancement of radiative recombination.

In this work, high-density InGaAs QDs with high optical quality grown above 450 °C are investigated. The best results were obtained by the introduction of p-type δ-doping in close proximity of the QD layer and subsequent post-growth annealing. With this new approach

a recovery dynamic of QD-SESAMs can be obtained similar to low-temperature grown QW-SESAMs but with a very high temperature insensitivity suitable for the monolithic integration into MIXSELs. The effect of different growth parameters, different types of p-doping and the influence of post-growth rapid thermal annealing (RTA) for these novel QD-SESAMs are discussed in detail.

2. SESAM growth and design

All SESAMs demonstrated in this paper were grown on semi-insulating GaAs (100) substrates by a Varian Gen II molecular beam epitaxy (MBE) system. The substrate temperature was measured during growth by a pyrometer. The high reflectivity DBR consists of 23 pairs of AlAs/GaAs quarter-wave layers grown at 605 °C with a designed stop band centered at 1030 nm (Fig. 1(a)). The InGaAs QD layers were formed by alternate deposition of InAs and $In_{0.2}Ga_{0.8}As$ layers with sub-monolayer thicknesses. In order to obtain the required QD layer thickness and thus the desired operation wavelength, the number of layer pairs had to be adjusted [19]. The GaAs layers after the DBR were grown at 590 °C, with the exception of the two 3 nm thick GaAs layers, which embed the QDs and were grown at their temperatures as given in Table 1. The position of the δ-doping layer (grown at 590 °C) for all SESAMs with a single QD layer is 3 or 5 nm after the QDs, respectively. For the SESAM with double QD layers there is one δ-doping layer before and one after the QDs (see elliptical insets in Fig. 1(a)). The total thickness of the absorber structure, which includes the GaAs barrier, QD layers and the last GaAs layer of the DBR, is about 220 nm. The QD layers are placed in an anti-node of the standing wave pattern of the electric field intensity. The influence of the growth temperature and indium content on the SESAM parameters were studied. For this purpose, the QD growth temperature was varied in the range of 450–480 °C and an indium content of 60% was used. Furthermore, the influence of post-growth RTA for 45 s at 650 °C on the recovery time was investigated. Figure 1(b) depicts an AFM scan of uncapped InGaAs QDs with an average indium content of 60% grown at 480 °C and a dot density of 1.0×10^{11} cm^{-2}.
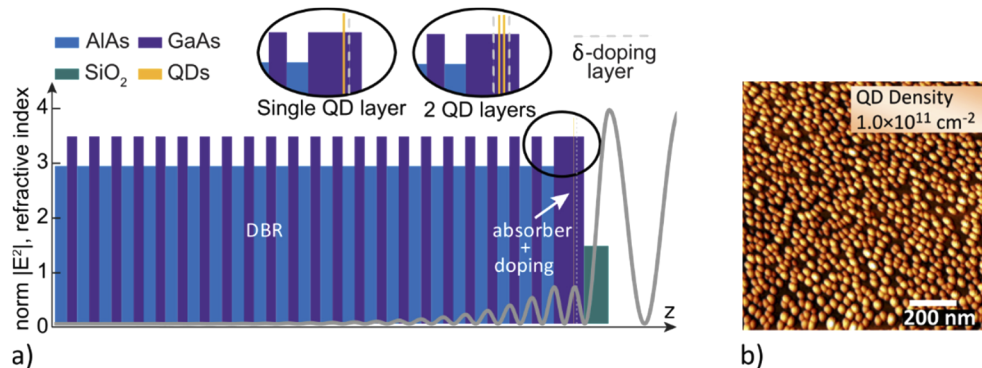

Fig. 1. a) Schematic layer stack of a complete QD-SESAM structure. Refractive index profile (colored as shown) and electric field intensity pattern at a wavelength of 1030 nm (grey). One or two QD layers and δ-doping were incorporated. b) AFM scan (1 × 1 μm^2) of $In_xGa_{1-x}As$ QDs grown at 480 °C with an indium content of 60% and a nominal deposited thickness of 1.4 nm.

The SESAM structure is designed for antiresonance, so the electrical field in the QD layer is less sensitive to small growth errors and wavelength changes compared to resonant structure, but it leads to larger saturation fluences and lower modulation depths (< 1%) [1,28]. The antiresonant structures yield flat, close to zero GDD, but they experience low field enhancement within the

Table 1. Summary of the MBE growth conditions for the absorber material and p-type beryllium δ-doping of all SESAMs used in this study. With SESAMs A - C the path towards the implementation of high quality and high dot density InGaAs QDs in the semiconductor absorber area has been explored. SESAMs D-F are used to investigate the influence of the beryllium δ-doping concentration on the recovery dynamics. SESAMs G and H were measured in an as-grown state and after post-growth RTA to investigate the influence of RTA on the recovery dynamics. Sample R is a state-of-the-art reference QW-SESAM with an 8-nm $In_{0.15}Ga_{0.85}As$ QW absorber embedded in AlAs barriers.

	Type of SESAM	Nominal thickness of absorber layers [nm]	Number of QD layers	Indium content [%]	Growth temperature [°C]	Number of doping layers	Doping density per doping layer [10^{12} cm^{-2}]	Doping distance [nm]	RTA
A	QD	1.4	1	60	400 °C	-	-	-	
B	QD	1.6	1	60	450 °C	1	0.1	5	
C	QD	1.4	1	60	480 °C	1	0.1	3	
D	QD	1.4	1	60	480 °C	1	0.1	5	
E	QD	1.4	1	60	480 °C	1	0.3	5	
F	QD	1.4	1	60	480 °C	1	2.0	5	
G	QD	1.4	1	60	480 °C	1	1.0	3	
H	QD	1.4	2	60	480 °C	2	1.0	3	
G*	QD	1.4	1	60	480 °C	1	1.0	3	45 s at 650 °C
H*	QD	1.4	2	60	480 °C	2	1.0	3	45 s at 650 °C
R	QW	8.0	-	15	280 °C	-	-	-	

structure. Therefore, after the semiconductor growth, an additional quarter-wave layer of fused silica was deposited with a temperature of around 300°C using plasma-enhanced chemical vapor deposition (PECVD) in order to enhance the standing electric field intensity pattern within the structure and thus increasing the saturation fluence still maintaining the desired broadband flat GDD characteristics [7]. Table 1 summarizes the MBE growth conditions for the absorber material and the p-type beryllium δ-doping of all SESAMs used in this study. Furthermore, it shows, for which samples post-growth annealing was used.

3. Methods

For morphological studies of the uncapped InGaAs QDs an atomic force microscope (AFM) (DME DS-95) was used. During photoluminescence (PL) measurements the grown samples were excited by a diode-pumped solid-state (DPSS) laser ($\lambda_{exc} = 532$ nm) and measured at 10 K with an excitation power density of about 21 W/cm^2.

The nonlinear reflectivity of the sample is characterized with the setup presented in [6], which has an accuracy of $< 0.05\%$ over a dynamic range of more than 4 orders of magnitude. According to the techniques described, the saturation fluence F_{sat} (i.e., the pulse fluence where the SESAM is saturated), the modulation depths ΔR (i.e., the difference in reflectivity between fully saturated and unsaturated SESAM) and the non-saturable losses ΔR_{ns} can be reliably determined.

The recombination dynamics are analysed in a custom pump-probe system presented in reference [15]. For a better comparison, the same Ti:Sapphire laser (repetition rate: 80 MHz; pulse duration: 140 fs; bandwidth: 12 nm at 1030 nm) is used for both measurement setups.

The recovery in semiconductor absorbers exhibit decay properties on two time scales and is best described by a double exponential decay

$$\Delta R_{pp}(\tau) = (A - 1)exp(-t/\tau_{slow}) + Aexp(-t/\tau_{fast}), \tag{1}$$

where ΔR_{pp} is the normalized pump-probe response [29]. The fast decay τ_{fast} with normalized amplitude A corresponds to intraband thermalization of the charge carriers in QW-SESAMS or fast inter-dot relaxation of excited states in QD-SESAMS. The slow component τ_{slow} is in both cases the result of a combination of interband recombination, carrier diffusion in the barriers, which are excited by two-photon absorption, and the carrier capture process into the QW or QD, respectively. In defect-free QW or QD material, the carrier recombination is mainly radiative and in the order of several 100 ps. Although the slow component limits the total response time, the impact can be much reduced if the amplitude A is near to 1. One representative number of the whole dynamics is the 1/e time constant $\tau_{1/e}$, which can be extracted from the fitting curve. In order to have a meaningful comparison between the samples, the normalized pump-probe response is fitted with Eq. (1) and all four parameters, i.e. the time constants τ_{fast}, τ_{slow}, $\tau_{1/e}$ and A are evaluated and compared.

4. Experimental results and discussion

4.1. Growth of high dot quality

The influence of the QD growth temperature on the recovery dynamics of the SESAMs was studied. SESAM R is used as a reference for the following investigations. It is a state-of-the-art MBE-grown fast QW SESAM [13,16], which consists of a single InGaAs QW absorber embedded in AlAs barriers and a comparable DBR (Fig. 2(a)).

As an initial QD-SESAM structure, a single undoped QD layer was grown at a low temperature of 400 °C. But instead of InAs QDs applied in previous studies [10,15,30], InGaAs QDs with an indium content of 60% were used (Sample A). At this low growth temperature, we expect a higher density of defects, which contribute to non-radiative recombination and which might be thermally unstable during high temperature overgrowth processes. Modulation depth and saturation fluence are on the order of magnitude of the QW reference sample and also the fast recovery component yields acceptable results (see table of Fig. 2(a)). However, the slow component of the recovery time is about seven times higher than that for the reference QW-SESAM and contribute more significantly to the overall dynamics as reflected by the low A value.

To obtain high optical quality temperature-stable QDs, higher QD growth temperatures are necessary. To see the impact of the growth temperature on the SESAM dynamics, two nominally identical QD-SESAMs (each optimized for 1030 nm) were grown at different growth temperatures (samples B, C grown at 450 °C and 480 °C, respectively). For these samples a beryllium δ-doping was already used to enhance the radiative recombination in the QDs. The significance and influence of the doping will be discussed in more detail in the next chapter.

In the left and middle column of Fig. 2(b) the AFM scans and corresponding height distribution histograms of QDs grown at 400°C, 450°C and 480°C comparable to the QDs used in the SESAMs are shown. The QD height distribution narrows with increasing growth temperature, whereby the average size is almost constant. In the right column, the photoluminescence spectra of samples A to C are presented. With increasing growth temperature, the emission intensity goes up significantly, which indicates the reduction of defects and the improved optical quality of the QDs and correlates well with the increased dot density. For SESAM B, grown at 450°C, a significantly reduced fast component and a moderate improvement on the slow time constant were obtained compared to sample A, grown at 400 °C. The overall larger $\tau_{1/e}$ value (13.5 ps) is a result of a reduced ratio between the fast and slow component (A = 0.47) and prevents an overall fast recovery of this SESAM. Also the PL measurement curve shows a small shoulder which may be caused by the observed bimodal dot distribution.

With a further increase of the growth temperature to 480 °C and a more efficient p-doping, it is possible to get a faster recovery dynamic but with low saturation fluence (see values in the table of Fig. 2(a). This proves that in principle fast recovery times can be obtained also at
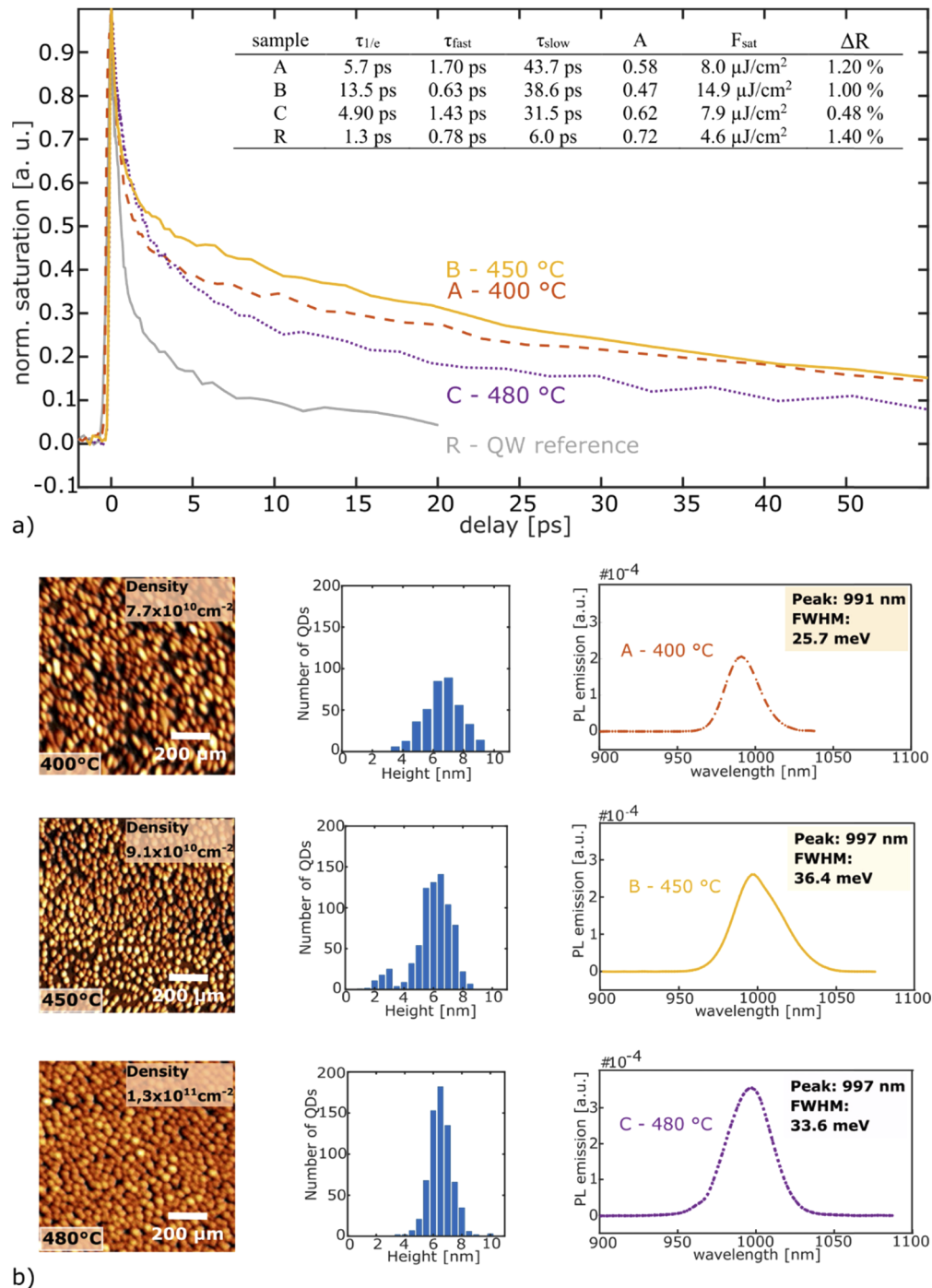
sample	$\tau_{1/e}$	τ_{fast}	τ_{slow}	A	F_{sat}	ΔR
A	5.7 ps	1.70 ps	43.7 ps	0.58	8.0 µJ/cm^2	1.20 %
B	13.5 ps	0.63 ps	38.6 ps	0.47	14.9 µJ/cm^2	1.00 %
C	4.90 ps	1.43 ps	31.5 ps	0.62	7.9 µJ/cm^2	0.48 %
R	1.3 ps	0.78 ps	6.0 ps	0.72	4.6 µJ/cm^2	1.40 %

Fig. 2. a) Pump-probe and F_{sat} measurement results of the reference QW-SESAM and three InGaAs QD-SESAM samples grown at 400 °C, 450 °C and 480 °C with an Indium content of 60% are shown. Both QD-SESAMs grown at higher temperature B and C are slightly δ-doped with an areal density of 1×10^{11} cm^{-2}. b) On the left side 1×1 µm^2 AFM scans of In$_x$Ga$_{1-x}$As QDs grown at 400°C, 450°C and 480 °C with an indium content of 60%, in the middle the corresponding height distribution histograms. The right side shows the low-temperature PL measurements of the QD-SESAMs. The thickness of QDs was optimized for a PL peak emission wavelength of 1030 nm at room temperature.

higher growth temperatures with p-doping. However, the $\tau_{1/e}$ value is still 4 times higher and the modulation depth ΔR is three times lower than the values for the QW reference sample.

For all subsequent samples, the growth temperature of QDs was kept at the desired value of 480 °C (see samples D to H in Table 1). The QDs thereby become less sensitive against annealing effects during growth but also contain fewer growth-dependent defects compared to low-temperature growth.

4.2. Beryllium doping

As mentioned in the introduction, the p-doping should enhance the radiative recombination of carriers in the electron ground state by modulation doping of the QDs via holes transfer from a Beryllium δ-doping layer nearby the QD layer as illustrated in Fig. 3(b).
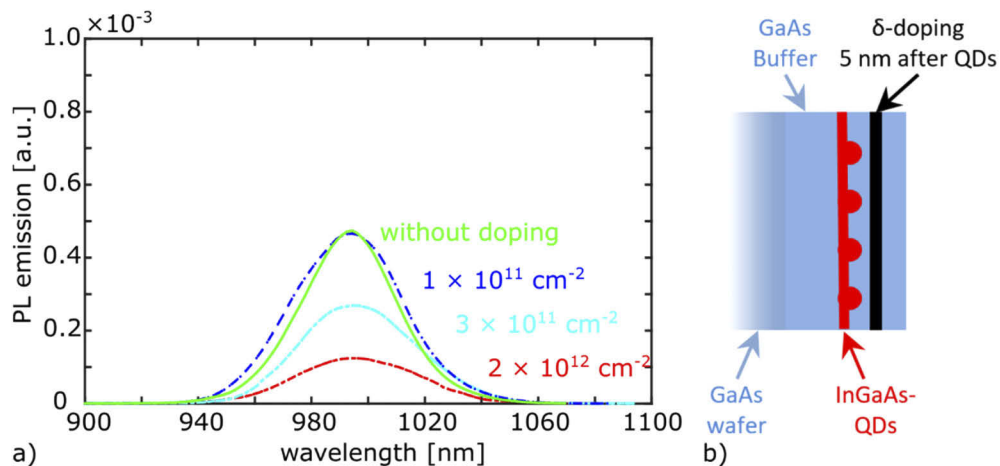

Fig. 3. a) PL spectra measured at 10 K of 1.4 nm nominally thick InGaAs QDs test samples undoped and with δ-doping (areal density was varied from 1×10^{11} cm^{-2} to 2×10^{12} cm^{-2} and a spacing of 5 nm) grown at 480 °C. b) The schematic layer stack of the test structure is identical with the absorber area of the SESAMs, except the DBR. The InGaAs QD-absorber layer and the δ-doping with beryllium at 5 nm after QDs are embedded in GaAs.

The intension is to get a high percentage of holes from the δ-doping layer to the QDs but to avoid an additional non-radiative recombination effect caused by the dopant impurity itself. Therefore, this is a trade-off between a short or large spacing and a high or low Beryllium areal density. Three different doping levels were chosen (1×10^{11} cm^{-2}, 3×10^{11} cm^{-2} and 2×10^{12} cm^{-2}) and a spacing of 5 nm to study the influence. With the lowest areal density of 1×10^{11} cm^{-2} and assuming a 100% charge transfer one should obtain about one hole per QD.

Figure 3(a) compares the PL spectra of InGaAs QD test samples with different doping levels and an undoped one. The structure of the test samples is identical with the absorber area of the SESAM, but without a DBR. A reduction of the PL peak intensity with increased doping concentration is clearly visible. This can be associated with enhanced non-radiative recombination of electron and holes in the QDs due to the spatial overlap of the carrier wave functions with crystal defects caused by the Beryllium doping. By increasing the Be doping also the defect density will increase. However, although this non-radiative effect will speed-up the depopulation of the QD ground states, this effect is not temperature-stable and will disappear after annealing or overgrowth at higher temperatures. This can be seen in the recovery of the integrated intensity shown in Fig. 5(b), which will be discussed in more detail in the following post-growth annealing section.

The saturation dynamics for the differently doped samples D – F relative to the QW reference sample is presented in Fig. 4. In comparison to sample C the distance between QDs and δ-doping was for all three samples 5 nm instead of 3 nm. The behavior looks more similar although a weak trend to faster response is visible with increasing doping level. In these non-annealed samples, the impact of defects in the barriers and the expected enhanced radiative recombination is difficult to be distinguished. However, an indication that the spacing between the δ-doping layer and the QD layer plays a significant role in these non-annealed SESAMs, can be clearly seen by comparing the dynamics of the nominally identical samples C and D but with different spacing values. With a smaller spacing (see sample C in Fig. 2(a)), the $\tau_{1/e}$ value of the recovery time is significantly reduced to half the value of sample D (see Fig. 4(a)). This effect can be explained by the exponentially dependent overlap of the electron wave function with the δ-doping layer. In addition, the hole transfer in the samples with larger spacings is also exponentially reduced. The enhancement of the radiative recombination by the hole modulation doping seems still minor in these non-annealed SESAMs.
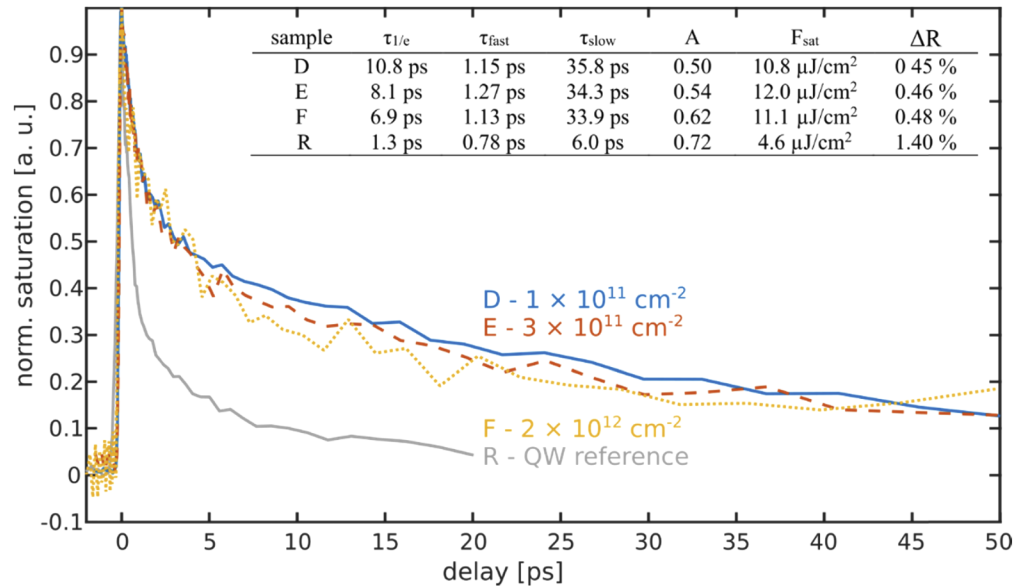

sample	$\tau_{1/e}$	τ_{fast}	τ_{slow}	A	F_{sat}	ΔR
D	10.8 ps	1.15 ps	35.8 ps	0.50	10.8 μJ/cm^2	0 45 %
E	8.1 ps	1.27 ps	34.3 ps	0.54	12.0 μJ/cm^2	0.46 %
F	6.9 ps	1.13 ps	33.9 ps	0.62	11.1 μJ/cm^2	0.48 %
R	1.3 ps	0.78 ps	6.0 ps	0.72	4.6 μJ/cm^2	1.40 %

Fig. 4. Pump-probe and F_{sat} measurement results of samples grown with different areal densities of the beryllium δ-doping (varied from 1×10^{11} cm^{-2} to 2×10^{12} cm^{-2}, 5 nm after QDs) to study the effect of doping concentration. All other parameters are kept constant (growth temperature of 480 °C with an indium content of 60%).

4.3. Rapid thermal annealing (RTA)

The effect of a post-growth RTA was used to increase the amplitude of the fast recovery *A* [31] and to achieve recovery times on the order of magnitude of the reference sample R. This allow a direct comparison between as-grown and annealed samples. By lowering the concentration of point defects with the annealing process [32], recombination within the QDs can be sped up [15,31].

To protect the surface, a SiO$_2$ cap was deposited by a chemical vapor phase deposition process, which is removed after RTA treatment by reactive ion etching (RIE) under fluorinated environments. To verify the annealing effect, a post-growth RTA step for 45 s at 650 °C (measured by a pyrometer) of all samples from Fig. 3(a) led to the PL measurements visualized in Fig. 5(a). The same trend for PL intensity could be observed as for the untreated samples. In addition, the

samples show different wavelength shifts dependent on the areal density of the beryllium doping. During annealing the porous SiO_2-cap layer acts as an effective sink for Ga out-diffusion (the thermal expansion coefficients of SiO_2 are ten times smaller than that of GaAs) [33,34]. Induced by the strain field a constant injection of Ga vacancies at the semiconductor surface happens. Also, the QD surface is under a significant compressive stress.
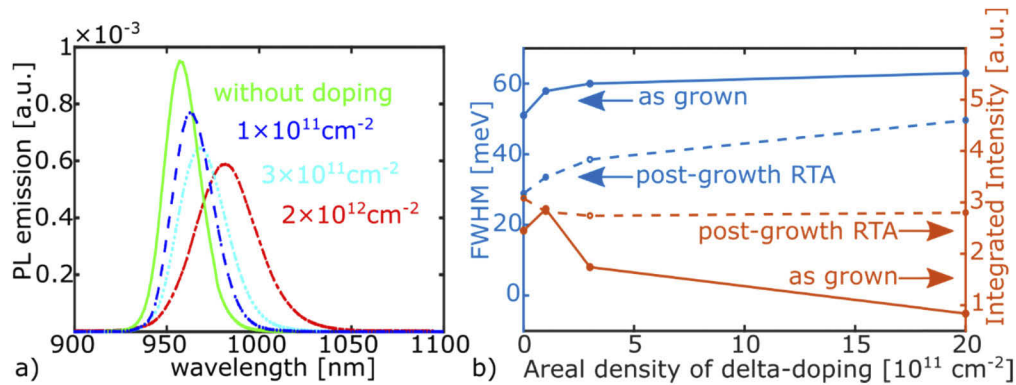

Fig. 5. a) PL spectra measured at 10 K of 1.4 nm nominally thick InGaAs QDs test samples undoped and with δ-doping (areal density was varied from 1×10^{11} cm^{-2} to 2×10^{12} cm^{-2}) grown at 480 °C. All samples were post-annealed for 45 s at 650 °C. b) Evaluation summary of PL FWHM and integrated intensity in dependence on the beryllium cell areal density for all the samples shown in a) and Fig. 3(a).

To release the stress, Ga atoms are promoted to interdiffuse into the InGaAs QD area. This results in a decrease of the indium concentration and hence an increase of the bandgap, resulting in a shift of the ground state transition to higher energies. The p-type doping influences the lateral diffusivity of the indium atoms of the QDs which compensates the interdiffusion of the Ga atoms [35]. Furthermore, with doping atoms diffusing into the QD layers gallium vacancies become neutralized. In fact, the p-doped QDs samples are much more temperature-stable and have notable insensitivity to intermixing caused by post growth annealing.

A higher shift in the wavelength is not expected during growth-related annealing in a MIXSEL structure. Compared to RTA both the temperature changes during MBE growth are much slower and the absolute growth temperature of 605 °C is lower which reduces the interdiffusion. The thermal stability of comparable high-quality InGaAs QDs grown at 480 °C has already been tested in MBE long-term growth of QD VECSEL structures [13].

In Fig. 5(b), the linewidth (FWHM) and the integrated intensities of the as grown samples from Fig. 3(a) (solid lines) and the post growth annealed samples from Fig. 5(a) (dashed lines) are plotted in dependence of the doping level. Both, the as-grown and annealed samples show a linewidth broadening with higher doping concentration. But the QD ensemble becomes more homogeneous during annealing, which in principle narrows the FWHM. After annealing the integrated intensity achieves a very similar level. For the highest doping level, the improvement is most severe. From this doping-level independent intensity behavior one can conclude that the majority of crystal defects are annealed and non-radiative recombination should not play any significant role anymore.

4.4. Optimized SESAMS with multiple QD layers

To further improve the dynamics, samples G and H with combined optimum parameters were grown, i.e., samples with a reduced spacing (3 nm) and a high doping level (1×10^{12} cm^{-2}). In optimum condition, this should result in a hole density of up to 10 holes per dot. To ensure a high

crystal and optical quality for an efficient charge transfer, the samples were also annealed with the same parameters discussed above. In addition, the impact of multiple QD layers is studied as well. For this purpose, sample H has two identical QD layers with nominal thicknesses of 1.4 nm grown at 480 °C, separated by a 15 nm GaAs barrier layer grown at 590 °C (i.e. to be precise first 3 nm GaAs at 480 °C and then continued with higher growth temperature) and a δ-doping 3 nm before and after the dots (see inset of Fig. 1(a)) each with an areal density of 1×10^{12} cm^{-2}. The total thickness of the QD absorber structure with the GaAs barriers was kept nearly constant.

In Fig. 6, the dynamics of the as-grown (G, H) and RTA-treated samples (G*, H*) are plotted. All samples except H* show a fast component of the recovery time below 1 ps quite comparable to the QW reference sample with 0.8 ps. However, the slow component decay rates of the as-grown structures are much higher and the $\tau_{1/e}$ value is about 10 times higher resulting in a low amplitude A.
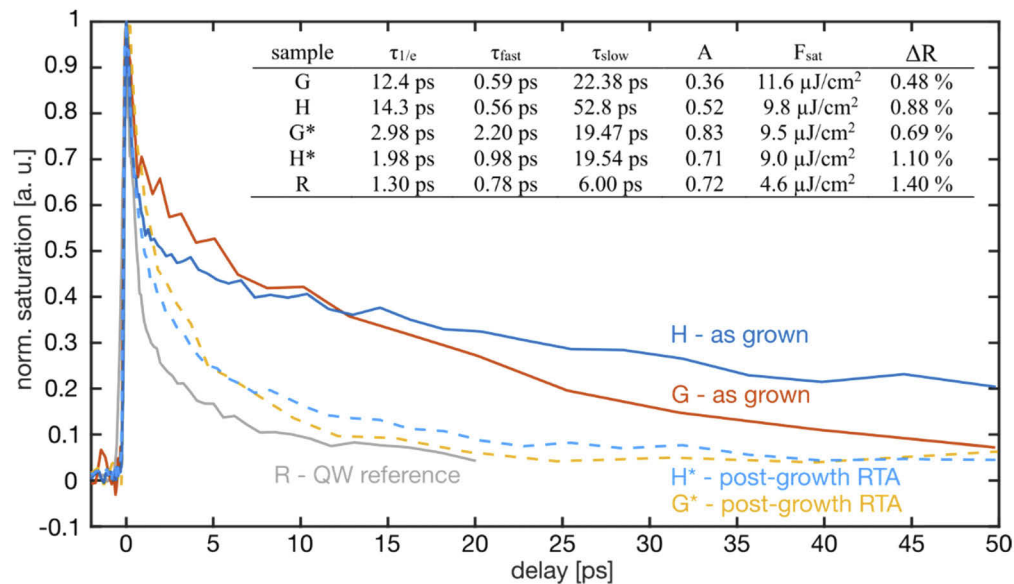

sample	$\tau_{1/e}$	τ_{fast}	τ_{slow}	A	F_{sat}	ΔR
G	12.4 ps	0.59 ps	22.38 ps	0.36	11.6 μJ/cm^2	0.48 %
H	14.3 ps	0.56 ps	52.8 ps	0.52	9.8 μJ/cm^2	0.88 %
G*	2.98 ps	2.20 ps	19.47 ps	0.83	9.5 μJ/cm^2	0.69 %
H*	1.98 ps	0.98 ps	19.54 ps	0.71	9.0 μJ/cm^2	1.10 %
R	1.30 ps	0.78 ps	6.00 ps	0.72	4.6 μJ/cm^2	1.40 %

Fig. 6. Pump-probe and F_{sat} measurement results of two SESAM samples (QDs grown at 480 °C with an indium content 60%) as-grown and treated with post-growth RTA are shown. The highly doped SESAM G/G* has one 1.4 nm nominally thick QD layer and a δ-doping 3 nm after the QD layer with an areal density of 1×10^{12} cm^{-2}. The SESAM H/H* has two 1.4 nm nominally thick QD layers and a δ-doping 3 nm before and after the QD layers each with an areal density of 1×10^{12} cm^{-2}.

From previous publications, it is already well known that with higher QD density and more absorber layers the modulation depth can be increased [15,28], but it affects also the recovery dynamics. An increased number of QD layers results usually in a longer recovery time. The $\tau_{1/e}$ value of both as grown samples G and H differs only slightly from 12 ps to 14 ps, but the slow component doubles as the number of QD layers increases from 1 to 2. With increasing QD areal density or higher number of QD layers the absorption increases [36,37].

Quite in contrast to that, the annealed samples show the best results. Although the annealed structures H* contain more absorber layers compared to the SESAMs from the previous chapters, recovery times below 20 ps for the slow component τ_{slow} were achieved for the first time in this study and the sample gets comparable to the single QW-SESAM. Further on, the normalized amplitude A of the fast decay τ_{fast} for sample H* is quite as high as for the reference sample R. Sample G* is even outperforming the reference sample with $A = 0.83$.

5. Summary

In conclusion, we have demonstrated the first antiresonant QD-SESAMs with high-quality $In_xGa_{1-x}As$/GaAs quantum dots and high-temperature stability suitable for the monolithic integration into MIXSEL devices. The effects of growth temperature, post-growth annealing, designs with single or double QD layer and different p-doping levels have been studied and the impact on the saturation parameters and the recovery dynamics were investigated. It could be experimentally demonstrated that the $\tau_{1/e}$ value of the recovery time can be adjusted to a level comparable to the reference QW-SESAM [13] by an optimized p-doping level close to the QD layer and a post-growth annealing step. This clearly demonstrates that the fast decay rates in saturable absorbers based on non-radiative recombination centers can be successfully substituted by enhanced radiative recombination in high optical quality QD absorbers using a p-type high-density modulation doping. With $\tau_{1/e}$ values below 2 ps, the recovery time reaches the level of QW absorbers grown at very low temperatures. Compared to QWs, QDs have the main advantage of a much larger parameter space for adapting and optimizing the functional parameters of a SESAM, such as saturation fluence (controlled by dot density, size and size distribution), operation wavelength range (related to much broader gain spectrum) and potential faster carrier dynamics (not yet realized). In addition, QD layers are much more stable towards built-in strain and defects, which allow for operation at high power levels or temperatures. We expect a significant improvement for the growth temperature stability and device performance by the integration of these new type of QD absorbers in MIXSEL structures.

Disclosures

The authors declare no conflicts of interest.

References

1. U. Keller, K. J. Weingarten, F. X. Kartner, D. Kopf, B. Braun, I. D. Jung, R. Fluck, C. Honninger, N. Matuschek, and J. aus der Au, "Semiconductor saturable absorber mirrors (SESAM's) for femtosecond to nanosecond pulse generation in solid-state lasers," IEEE J. Sel. Top. Quantum Electron. **2**(3), 435–453 (1996).
2. U. Keller, "Recent developments in compact ultrafast lasers," Nature **424**(6950), 831–838 (2003).
3. M. H. Ober, M. Hofer, U. Keller, and T. H. Chiu, "Self-starting, diode-pumped femtosecond Nd fiber laser," Opt. Lett. **18**(18), 1532 (1993).
4. U. Keller and A. C. Tropper, "Passively modelocked surface-emitting semiconductor lasers," Phys. Rep. **429**(2), 67–120 (2006).
5. B. W. Tilma, M. Mangold, C. A. Zaugg, S. M. Link, D. Waldburger, A. Klenner, A. S. Mayer, E. Gini, M. Golling, and U. Keller, "Recent advances in ultrafast semiconductor disk lasers," Light: Sci. Appl. **4**(7), e310 (2015).
6. D. J. Maas, B. Rudin, A.-R. Bellancourt, D. Iwaniuk, S. V. Marchese, T. Südmeyer, and U. Keller, "High precision optical characterization of semiconductor saturable absorber mirrors," Opt. Express **16**(10), 7571–7579 (2008).
7. G. J. Spühler, K. J. Weingarten, R. Grange, L. Krainer, M. Haiml, V. Liverini, M. Golling, S. Schön, and U. Keller, "Semiconductor saturable absorber mirror structures with low saturation fluence," Appl. Phys. B **81**(1), 27–32 (2005).
8. M. Mangold, C. A. Zaugg, S. M. Link, M. Golling, B. W. Tilma, and U. Keller, "Pulse repetition rate scaling from 5 to 100 GHz with a high-power semiconductor disk laser," Opt. Express **22**(5), 6099–6107 (2014).
9. D. J. H. C. Maas, A.-R. Bellancourt, B. Rudin, M. Golling, H. J. Unold, T. Südmeyer, and U. Keller, "Vertical integration of ultrafast semiconductor lasers," Appl. Phys. B **88**(4), 493–497 (2007).
10. E. U. Rafailov, A. A. Lagatsky, S. A. Zolotovskaya, and W. Sibbett, "Compact and efficient mode-locked lasers based on QD-SESAMs," Proc. SPIE **6998**, 69980B (2008).

11. D. Lorenser, D. J. H. C. Maas, H. J. Unold, A.-R. Bellancourt, B. Rudin, E. Gini, D. Ebling, and U. Keller, "50-GHz Passively Mode-Locked Surface-Emitting Semiconductor Laser With 100-mW Average Output Power," IEEE J. Quantum Electron. **42**(8), 838–847 (2006).

12. M. Hoffmann, O. D. Sieber, V. J. Wittwer, I. L. Krestnikov, D. A. Livshits, Y. Barbarin, T. Südmeyer, and U. Keller, "Femtosecond high-power quantum dot vertical external cavity surface emitting laser," Opt. Express **19**(9), 8108–8116 (2011).

13. C. G. E. Alfieri, D. Waldburger, M. Golling, and U. Keller, "High-Power Sub-300-Femtosecond Quantum Dot Semiconductor Disk Lasers," IEEE Photonics Technol. Lett. **30**(6), 525–528 (2018).

14. B. Rudin, V. J. Wittwer, D. J. H. C. Maas, M. Hoffmann, O. D. Sieber, Y. Barbarin, M. Golling, T. Südmeyer, and U. Keller, "High-power MIXSEL: an integrated ultrafast semiconductor laser with 6.4 W average power," Opt. Express **18**(26), 27582–27588 (2010).

15. D. J. H. C. Maas, A.-R. Bellancourt, M. Hoffmann, B. Rudin, Y. Barbarin, M. Golling, T. Südmeyer, and U. Keller, "Growth parameter optimization for fast quantum dot SESAMs," Opt. Express **16**(23), 18646–18656 (2008).

16. M. Mangold, V. J. Wittwer, C. A. Zaugg, S. M. Link, M. Golling, B. W. Tilma, and U. Keller, "Femtosecond pulses from a modelocked integrated external-cavity surface emitting laser (MIXSEL)," Opt. Express **21**(21), 24904–24911 (2013).

17. M. Mangold, M. Golling, E. Gini, B. W. Tilma, and U. Keller, "Sub-300-femtosecond operation from a MIXSEL," Opt. Express **23**(17), 22043–22059 (2015).

18. E. U. Rafailov, S. J. White, A. A. Lagatsky, A. Miller, W. Sibbett, D. A. Livshits, A. E. Zhukov, and V. M. Ustinov, "Fast Quantum-Dot Saturable Absorber for Passive Mode-Locking of Solid-State Lasers," IEEE Photonics Technol. Lett. **16**(11), 2439–2441 (2004).

19. T. Finke, V. Sichkovskyi, and J. P. Reithmaier, "Optimization of size uniformity and dot density of InxGa1−xAs/GaAs quantum dots for laser applications in 1 µm wavelength range," J. Cryst. Growth **517**, 1–6 (2019).

20. X. Wang, Y. J. Zhu, C. Jiang, Y. X. Guo, X. T. Ge, H. M. Chen, J. Q. Ning, C. C. Zheng, Y. Peng, X. H. Li, and Z. Y. Zhang, "InAs/GaAs quantum dot semiconductor saturable absorber for controllable dual-wavelength passively Q-switched fiber laser," Opt. Express **27**(15), 20649–20658 (2019).

21. K. P. Korona, "Arsenic Antisite Defects Correlations in Low Temperature MBE GaAs," Acta Phys. Pol., A **88**(4), 643–653 (1995).

22. D. Sreenivasan, J. E. M. Haverkort, T. J. Eijkemans, and R. Nötzel, "Photoluminescence from low temperature grown InAs/GaAs quantum dots," Appl. Phys. Lett. **90**(11), 112109 (2007).

23. M. Haiml, U. Siegner, F. Morier-Genoud, U. Keller, M. Luysberg, R. C. Lutz, P. Specht, and E. R. Weber, "Optical nonlinearity in low-temperature-grown GaAs: Microscopic limitations and optimization strategies," Appl. Phys. Lett. **74**(21), 3134–3136 (1999).

24. M. Haiml, U. Siegner, F. Morier-Genoud, U. Keller, M. Luysberg, P. Specht, and E. R. Weber, "Femtosecond response times and high optical nonlinearity in beryllium-doped low-temperature grown GaAs," Appl. Phys. Lett. **74**(9), 1269–1271 (1999).

25. U. Siegner, M. Haiml, F. Morier-Genoud, R. C. Lutz, P. Specht, E. R. Weber, and U. Keller, "Femtosecond nonlinear optics of low-temperature grown semiconductors," Phys. B **273-274**, 733–736 (1999).

26. Sercel, "Multiphonon-assisted tunneling through deep levels: A rapid energy-relaxation mechanism in nonideal quantum-dot heterostructures," Phys. Rev. B **51**(20), 14532–14541 (1995).

27. H. Ye, L. Li, R. T. Hinkey, R. Q. Yang, T. D. Mishima, J. C. Keay, M. B. Santos, and M. B. Johnson, "MBE growth optimization of InAs (001) homoepitaxy," J. Vac. Sci. Technol., B: Nanotechnol. Microelectron.: Mater., Process., Meas., Phenom. **31**(3), 03C135 (2013).

28. A.-R. Bellancourt, Y. Barbarin, D. J. H. C. Maas, M. Shafiei, M. Hoffmann, M. Golling, T. Südmeyer, and U. Keller, "Low saturation fluence antiresonant quantum dot SESAMs for MIXSEL integration," Opt. Express **17**(12), 9704–9711 (2009).

29. D. J. H. C. Maas, *MIXSELs - a new class of ultrafast semiconductor lasers*. Zugl.: Zürich, Techn. Hochsch., Diss., 2008, 1. ed. (Hartung-Gorre, 2009).

30. M. Hoffmann, Y. Barbarin, D. J. H. C. Maas, M. Golling, I. L. Krestnikov, S. S. Mikhrin, A. R. Kovsh, T. Südmeyer, and U. Keller, "Modelocked quantum dot vertical external cavity surface emitting laser," Appl. Phys. B **93**(4), 733–736 (2008).

31. D. J. H. C. Maas, A.-R. Bellancourt, M. Hoffmann, B. Rudin, M. Golling, T. Sudmeyer, and U. Keller, "Recombination dynamics in quantum dot semiconductor saturable absorber Mirrors (QD-SESAMs)," in *Lasers and Electro-Optics, 2008 and 2008 Conference on Quantum Electronics and Laser Science. CLEO* (IEEE, 2008), pp. 1–2.

32. W. H. Jiang, H. Z. Xu, B. Xu, X. L. Ye, J. Wu, D. Ding, J. B. Liang, and Z. G. Wang, "Annealing effect on the surface morphology and photoluminescence of InGaAs/GaAs quantum dots grown by molecular beam epitaxy," J. Cryst. Growth **212**(4), 356–359 (2000).

33. H. S. Djie, O. Gunawan, D.-N. Wang, B. S. Ooi, and J. C. M. Hwang, "Group-III vacancy induced InxGa1−xAs quantum dot interdiffusion," Phys. Rev. B **73**(1-2), 154 (2006).

34. L. Fu, J. Wong-Leung, P. N. K. Deenapanray, H. H. Tan, C. Jagadish, B. Gong, R. N. Lamb, R. M. Cohen, W. Reichert, L. V. Dao, and M. Gal, "Suppression of interdiffusion in GaAs/AlGaAs quantum-well structure capped with dielectric films by deposition of gallium oxide," J. Appl. Phys. **92**(7), 3579–3583 (2002).

35. Y. Qiu, Z. Y. Zhang, R. A. Hogg, A. G. Cullis, and T. Walther, "Study of annealed InAs/GaAs quantum dot structures," J. Phys.: Conf. Ser. **209**, 012036 (2010).

36. E. U. Rafailov, M. A. Cataluna, and E. A. Avrutin, *Ultrafast Lasers Based on Quantum Dot Structures. Physics and Devices*, 1. Aufl. (Wiley-VCH, 2011).

37. A. E. Abouelez, E. Eldiwany, M. B. El Mashade, and H. A. Konber, "Modelling and simulation of p-i-n quantum dot semiconductor saturable absorber mirrors," Prog. Electromagn. Res. C **82**, 39–53 (2018).